Quantum Electronics **46** (5) 473–480 (2016)

LASER-PLASMA SOURCE OF EUV RADIATION DOI: 10.1070/QEL16019

High-brightness EUV source based on laser plasma using a liquid-metal droplet target

A.Yu. Vinokhodov, M.S. Krivokorytov, Yu.V. Sidelnikov, V.M. Krivtsun, V.V. Medvedev, K.N. Koshelev

Abstract. **We present the study of a source of extreme ultraviolet (EUV) radiation based on laser plasma generated due to the interaction of radiation from a nanosecond Nd : YAG laser with a liquid-metal droplet target consisting of a low-temperature eutectic indium–tin alloy. The generator of droplets is constructed using a commercial nozzle and operates on the principle of forced capillary jet decomposition. Long-term spatial stability of the centre-of-mass position of the droplet with the root-mean-square deviation of ~0.5 μm is demonstrated. The use of a low-temperature working substance instead of pure tin increases the reliability and lifetime of the droplet generator. For the time- and space-averaged power density of laser radiation on the droplet target 4×10^{11} W cm^{-2} and the diameter of radiating plasma ~80 μm, the mean efficiency of conversion of laser energy into the energy of EUV radiation at 13.5 ± 0.135 nm equal to 2.3% $(2\pi$ sr$)^{-1}$ is achieved. Using the double-pulse method, we have modelled the repetitively pulsed regime of the source operation and demonstrated the possibility of its stable functioning with the repetition rate up to 8 kHz for the droplet generation repetition rate of more than 32 kHz, which will allow the source brightness to be as large as ~0.96 kW (mm^2 sr)$^{-1}$.**

Keywords: *EUV lithography, actinic EUV source, laser plasma, Nd : YAG laser, generator of liquid-metal droplets, laser target, spatial stability, conversion efficiency, source brightness, EUV radiation spectrum.*

1. Introduction

At present, the evolutionary development of projection lithography has changed for novel revolutionary technologies. The transition occurred from UV sources – excimer lasers with the wavelengths $\lambda = 248$ and 193 nm – to plasma sources of extreme ultraviolet (EUV) radiation with $\lambda = 13.5 \pm 0.135$ nm (in-band range), and, correspondingly, from refracting projection optics to reflecting optics based on Bragg mirrors [1], which is due to the fact that the traditional optical lithography, even using additional technologies (immersion optics, multiple photoresist exposure) has approached the limit of optical resolution $\delta \approx 22$ nm. At the same time, the EUV lithography allows the chip fabrication with the scale much smaller than $\delta = 10$ nm [2]. However, the transition to EUV lithography requires also new instruments for diagnostics of the used masks, fabricated on the basis of multilayer reflecting coatings. The main method used for this purpose is the scanning of the mask surface with actinic EUV radiation with the wavelength $\lambda = 13.5$ nm, which is explained by a strong dependence of the scattered radiation intensity on the source wavelength ($\sim 1/\lambda^4$). The source of such radiation must have high brightness B, equal to a few hundred W (mm^2 sr)$^{-1}$ and a small geometric factor of the collector system $E = 10^{-3}$–10^{-4} mm^2 sr [3].

In the present paper, we report the continuation of our studies on fabricating a high-brightness source of EUV radiation for diagnostics of masks in EUV lithography. In our previous paper [4], we presented the results of the study of a high-brightness EUV source based on the laser-induced discharge plasma (DPP) produced between liquid-metal electrodes. Although in [4] we showed the possibility of obtaining high [~200W (mm^2 sr)$^{-1}$] values of the source brightness and unlimited lifetime of electrodes, the problem of a 'clean' source, i.e., the problem of removing a large amount of plasma reaction products (PRP) that pollute the collector mirror and reduce its lifetime, was not solved. Besides that, the attained energy stability of the EUV source from pulse to pulse $\sigma_0 \geqslant 13\%$ (σ_0 being the relative root-mean-square deviation of the EUV pulse energy) was far from the values required for such a source ($\sigma_0 = 1\%$–3%). The poor stability of the EUV source was mainly due to the poor reproducibility of the surface profile of jet electrodes, onto which the initiating laser radiation was focused, which lead to fluctuations of the discharge parameters and, as a result, of the output parameters of EUV radiation.

The aim of the present work is to study the possibility of designing a high-brightness EUV source based on the LPP method, i.e. an alternative method of generating a high-temperature plasma using focused laser radiation, when a droplet of tin plays the role of a target [5, 6]. Compared to the DPP sources, in the LPP ones it is easier to produce radiation with high brightness, the amount of which is inversely proportional to the area of the radiating plasma within the solid angle of the optical collector. In the case of the LPP source, this area is determined either by the size of the focused laser radiation, or by the diameter of the target droplet (depending on the ratio of these sizes). Using a Nd : YAG laser with good beam quality, the laser caustic diameter can be made smaller than 100 μm, while the characteristic size of the discharge plasma radiating in the EUV range amounts to 200–300 μm

A.Yu. Vinokhodov, M.S. Krivokorytov 'EUV Labs' Ltd., Sirenevyi blvd. 1, Troitsk, 142190 Moscow, Russia; e-mail: avinokhod@gmail.com;
Yu.V. Sidelnikov, V.M. Krivtsun, V.V. Medvedev, K.N. Koshelev Institute of Spectroscopy, Russian Academy of Sciences, ul. Fizicheskaya 5, Troitsk, 142190 Moscow, Russia; 'EUV Labs' Ltd., Sirenevyi blvd. 1, Troitsk, 142190 Moscow, Russia;
e-mail: krivtsun@isan.troitsk.ru

Received 19 January 2016
Kvantovaya Elektronika **46** (5) 473–480 (2016)
Translated by V.L. Derbov

and more [4, 7]. In the studied source, the role of the target is played by a droplet with the diameter, close to that of the focused laser radiation. Such a target with the limited mass allows minimisation of the PRP amount. The working substance of the droplet is a low-temperature tin-containing eutectic In/Sn alloy. On the one hand, it efficiently radiates in the in-band range provided that the parameters of the laser plasma are appropriate (similar to pure tin), and, on the other hand, due to using a lower operating temperature than in the case of pure tin, it facilitates more reliable operation of the droplet generator and, therefore, the entire source.

In contrast to LPP EUV sources radiation that are used in lithography for serial chip production [high volume manufacturing (HVM)], in the actinic LPP sources, intended for metrology, there is no need to use complex and expensive pre-pulse technology [8]. In the HVM technology the role of the pre-pulse is, first, to expand the target to the size matching the caustic diameter of the focused CO_2 laser radiation, which amounts to no less than 200 μm, before the impact of the main laser pulse. Second, the pre-pulse allows obtaining a fragmented target that better absorbs the laser radiation and is better 'burned' by the main laser pulse. However, using the Nd:YAG laser as the main one, the diameter of the focused radiation will be initially matched with the diameter of the droplet, and for efficient interaction of laser radiation with the target it is not necessary to increase the size of the latter. On the other hand, in a high-brightness EUV source the achievement of record-breaking values of the conversion efficiency η of laser energy to that of the in-band radiation plays no crucial role, and the required brightness is achieved in LPP sources even at $\eta \approx 1\%-1.5\%$ and repetition rates $f = 10$ kHz and lower [9]. Thus, the concept of a high-brightness LPP source developed by us, as in Ref. [9], is based on a single Nd:YAG laser and a liquid-metal droplet target made of a low-temperature alloy.

2. Experimental setup

The scheme of the experimental setup shown in Fig. 1 is largely similar to that used by us in Ref. [10], where the dynamics of droplet deformation under the action of femto- and picosecond laser pulses was investigated. The experimental setup incorporated a vacuum chamber (*1*), a generator of liquid-metal droplets (*2*), a Nd:YAG-based laser system (*3*), a system of synchronisation and diagnostic equipment. The vacuum chamber had 22 diagnostic pipes placed at different angles to the optical axis of the Nd:YAG laser, and was evacuated by means of a turbomolecular pump to the residual gas pressure smaller than 10^{-4} mbar. The droplet generator was placed in the centre of the upper flange of the vacuum chamber (shown in Fig. 1 by a dashed-line circle); the droplet velocity vector is directed perpendicular to the plane of the figure. The synchronisation system provided fitting of the droplet with the laser pulse. In the experiment, we used the diagnostic equipment that may be conditionally divided into three groups for diagnostics of the laser radiation, the droplet target and its fragments, and the EUV radiation.

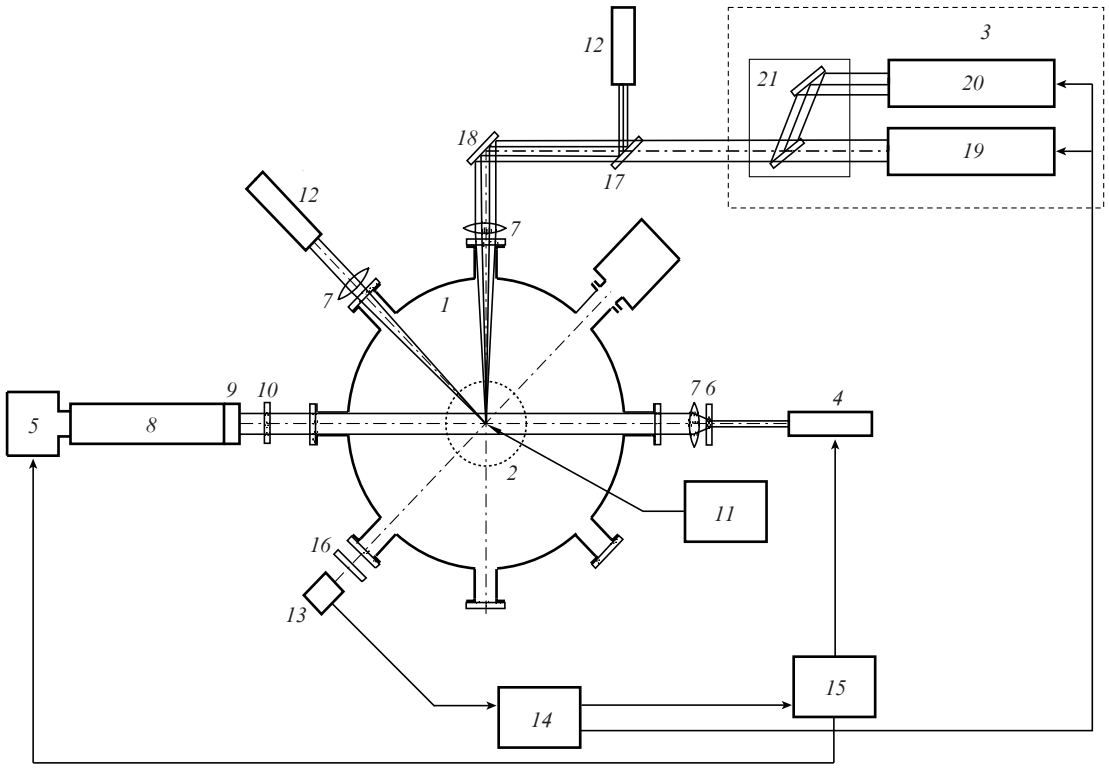

Figure 1. Schematic of the setup: (*1*) vacuum chamber; (*2*) droplet generator; (*3*) Nd:YAG laser system; (*4*) illuminating diode laser; (*5*) CCD video camera; (*6*) optical diffusor; (*7*) focusing lenses; (*8*) microscope; (*9*) objective; (10) narrow-band filter ($\lambda = 850$ nm); (*11*) control unit of the droplet generator; (*12*) cw visible-range lasers; (*13*) photodiode with amplifier; (*14*) detector of signal maximum with frequency divider; (*15*) delay generator; (*16*) narrow-band filter ($\lambda = 660$ nm); (*17*) wedge; (*18*) mirror; (*19*) first unit of the Nd:YAG laser; (*20*) second unit of the Nd:YAG laser; (*21*) beam convergence device.

2.1. Generator of liquid-metal droplets

The generator of liquid-metal droplets incorporated a heated tank with liquid metal, equipped with a system of vacuuming and supplying the controlled pressure of gas (argon), and the capillary nozzle assembly, consisting of a nozzle and a filter based on sintered metallic powder. The tank of the droplet generator was made of molybdenum that weakly interacts with the liquid tin and its eutectic alloys at the working temperatures lower than 250 °C. The generator included the commercial nozzle (Microfab Technologies) with a ring piezoelectric element (actuator) to implement the droplet generation with the specified repetition rate. The electric capacity of the ring actuator amounted to 2–3 nF, and the diameter of the outlet hole of the nozzle was equal to 20, 30, or 40 μm.

In contrast to Ref. [10], in this work we used only the jet regime of the nozzle operation, in which the pressure in the tank with liquid metal significantly exceeds the capillary pressure in the nozzle. As a result, at the outlet of the nozzle a jet is formed that due to the Rayleigh instability decomposes into droplets at a certain distance from the nozzle, depending on the applied pressure. When AC voltage is applied to the piezoelectric ring, the induced modulation of the jet decomposition occurs with the given frequency. The droplet diameter in our experiments varied from 33 to 90 μm depending on the outlet diameter of the nozzle, the velocity of the droplets and the rate of their repetition.

While in Ref. [10] only one filter was used to filter the working substance, in the present modification of the droplet generator three filters made of sintered medal powder are installed in sequence, with the filtering fineness 20, 10 and 5 μm. This facilitated more stable operation of the droplet generator. The tank and the nozzle unit were equipped with an automated system keeping the temperature constant.

As in Ref. [10], the eutectic In/Sn alloy with the mass composition of 0.52/0.48 played the role of the working substance. Using this alloy provides the efficiency of conversion in the LPP EUV sources close to that with pure tin, but the melting temperature of the alloy (119 °C) is much lower than that of tin (232 °C). The lower operating temperature, first, facilitates more reliable and long-term operation of the nozzle unit of the droplet generator, and, second, reduces the solubility of construction materials in the working substance, thus preventing its pollution.

2.2. Droplet diagnostics and synchronisation system

For the diagnostics of spatial stability of the position of droplets, the method of shadow photography in weakly divergent laser light was used. The region of interaction of laser radiation with the droplet target and, therefore, the region of the droplet target diagnostics, was located at the distance of 45 mm from the nozzle. As the illuminating source a pulsed diode laser (*4*) (IL30C) (Fig. 1) with $\lambda = 850$ nm and pulse duration 30 ns was used. The shadow image of the droplets was recorded by the matrix of a CCD camera (*5*) (Manta MG-145B). The uniformity of the illumination field was provided by an optical diffusor (*6*) with a scattering angle 20° and a positive lens (*7*). The microscope (*8*) (DisteMax Model K2) and the objective (*9*) with the $2^{\times}$ magnification projected the droplet image on the CCD matrix of the video camera. The diagnostics of droplets was performed in two directions: in the direction transverse to the optical axis of the main laser beam and at a small angle (17°) to it. Besides, for the diagnostics of the process of droplet formation near the nozzle the second channel of shadow photography was used, including the same elements as the first one, i.e., the illuminating laser, the microscope and the video camera. The elements of this channel are not shown in Fig.1.

In the course of recording shadow photographs the background illumination before the microscope was cut off using a narrow-band filter (*10*) with the transmission band $\Delta\lambda = 850 \pm 5$ nm. The camera field of view was 3.2×2.4 mm, and the resolution was 2.3 μm. The maximal rate of recording the full field of view was 15 s^{-1}. If the operation of the droplet generator is stable, all droplets will have the same velocities and trajectories of flight. In the case of synchronous operation of the stable generator of droplets and the illuminating laser pulse, the computer monitor reproduces an immovable image of drops due to the stroboscopic effect. After recording a series of frames, one can measure the spatial stability of the droplet position in two directions, the longitudinal and the transverse one, with respect to the droplet velocity vector.

Due to the pressure drift or temperature variations in the tank with the working substance and in the nozzle unit, as well as the mechanical particles present in the working substance, the velocity of droplets may fluctuate. Therefore, to provide stable hitting of laser radiation into the droplet target, the system of synchronisation was used, in which the main Nd:YAG laser and the delay generator, controlling the diagnostic lasers and CCD cameras, was triggered by the target droplet when it was slightly above the point of interaction between the laser pulse and the droplet. In this synchronisation system, the droplet generator, clocked by a separate generator (*11*), operates with the given rate of pulse repetition independent of other elements of the synchronisation system. The triggering from the target droplet is implemented by means of a cw visible-range laser ($\lambda = 662$ nm) (*12*), the radiation from which is focused by a lens (*7*) onto the axis of the droplet flight. Passing through the beam of the cw laser radiation, the droplets reflect it, and the reflected light is detected at a certain angle by a photodiode (*13*). Via the transimpedance amplifier, the signal is applied to the unit (*14*) that forms synchropulses corresponding to the maxima of the diode signal. These pulses are then divided and used to trigger the main laser and the system of droplet diagnostics [diagnostic lasers (*4*) and CCD cameras (*5*)]. While for triggering the main laser the coefficient of division was varied within the range 2–10, for triggering the delay generator (*15*) it was equal to 10000.

To provide stable operation of the synchronisation system at a high laser pulse repetition rate, a narrow-band filter (*16*) with $\Delta\lambda = 660 \pm 5$ nm was installed in front of the photodiode, which cut off the most part of the laser plasma radiation, so that to the moment of the next laser pulse the photodiode was not in the saturated state. The minimal delay between the moment of detection of the signal reflected from the droplet and the moment of the main laser pulse amounts to ~8 μs. This time actually determines the longitudinal stability of the droplet location in the direction of its velocity vector. By varying the delays between the pulses of the main laser and the illuminating one, as well as the moment of opening the frame of the CCD camera, one can record the spread of the droplet fragments at different time delays with respect to the main laser pulse. To adjust the radiation of the main Nd:YAG laser at the droplet we used an auxiliary visible-range laser (*12*), for which the beam axis was converged with that of the main Nd:YAG laser by means of a wedge (*17*). By aligning

the last mirror (*18*), the beam of the auxiliary laser (*12*) was adjusted at the axis of droplet flight. The ultimate adjustment of the laser beam at the droplet was performed using the images of the spreading fragments of the target; for this aim with some delay (usually 2–3 μs) the symmetric shape of fragments in both mutually perpendicular directions was achieved by aligning the mirror (*18*).

2.3. Laser system

In the experiments, we used the doubled laser system LS-2147D-L-FF based on Nd:YAG lasers LS-2147/2. The maximal pulse energy at the target for the laser units (*19*) and (*20*) (Fig. 1) achieved $E_{las} \approx 180$ mJ, the pulse duration at the half-maximum intensity level was $\Delta\tau \approx 18$ ns and the maximal pulse repetition rate was 10 Hz. The beams of laser radiation were converged to a single optical axis by means of a convergence device (*21*). The laser radiation energy was measured with a calorimetric Gentec UP-55-300F-H12 head and a Maestro indicator. The analysis of the focal spot image, obtained by means of a Spiricon SP-620 beam profile meter, has shown that the power density distribution in the laser beam is regular and close to Gaussian in both mutually perpendicular directions. The caustic diameters at the half-maximum intensity level was equal to ~50 μm using the lens with the focal length $F = 290$ mm. Thus, the mean power density of laser radiation at the target was $P \approx 4 \times 10^{11}$ W cm^{-2}. The use of the doubled laser system allowed modelling of the repetitively pulsed regime of the source operation with a high pulse repetition rate. The delay of the second laser pulse with respect to the first one modelled the pulse repetition rate within the frequency range of interest 5–10 kHz. Since the output parameters of the laser units were slightly different in energy and pulse duration, they were tuned so that under the impact of each unit on the droplet target the level of the EUV signal was the same.

2.4. Diagnostics of EUV radiation

The absolute measurement of the EUV pulse energy was implemented using the AXUV-100 photodiode with a multilayer Zr/Si filter deposited on its surface and the spectrometer. Before the arrival at the photodiode, the radiation from plasma was reflected from the multilayer 45-degree Zr/Si mirror with the reflection coefficient 25% at the wavelength $\lambda = 13.5$ nm. Thus, in the channel the double spectral filtering of the plasma radiation was implemented. The integral spectral transmission band of the entire measurement channel amounted to 13.1–13.8 nm. The procedure of calculating the absolute energy of the EUV radiation pulses was the following. The spectrum of the laser plasma radiation was measured in the EUV range from 5 to 20 nm and the convolution of the Zr/Si filter transmission spectrum, the Zr/Si mirror reflection spectrum and the laser plasma spectrum was calculated. Then using the obtained spectral dependence, we calculated the fraction of in-band energy with respect to the total energy passed through the measurement channel. In our case it was 56.5%. With the known calibration coefficient of the AXUV-100 photodiode, equal to 0.19 K J^{-1}, and the coefficients of the mirror reflection and filter transmission, we calculated the ultimate value of energy of the in-band radiation.

The radiation spectrum of the laser plasma was measured using the GS-2 spectrometer (X-Meter). This is a gliding-incidence spectrometer with the spectral range 3–60 nm and relative resolution $\lambda/\delta\lambda = 300$. The diffraction grating (600 lines mm^{-1}) and the slit 40 μm wide were used in the spectrometer.

The dimensions of the plasma region radiating in the EUV range were measured using a CS-8300 CCD camera (TELI) with a deposited layer of a luminophore sensitive to the EUV radiation, and a camera obscura with a pinhole diameter of 40 μm. In front of the CCD camera, a zirconium foil filter was installed to provide the spectral transmission band of the channel 5–21 nm. The results were processed using the MrBeam 3.2.2 programme.

3. Experimental results and discussion

3.1. Target

To generate stable pulses of EUV radiation it is necessary, first of all, to provide stable spatial position of the droplet target from pulse to pulse. The stable regime of the droplet generator operation was observed at the rate of droplet repetition $n = 20$–125 kHz. The maximal velocity of droplets, which in our experiments did not exceed 15 m s^{-1}, determined the upper limit of this range. The best results for the spatial stability of droplets were achieved within a narrower range of repetition rates $n = 30$–65 kHz. Figure 2 presents the photographs of sequences of droplets with different diameters, obtained using the nozzle with the outlet diameter 20 μm and different n values.

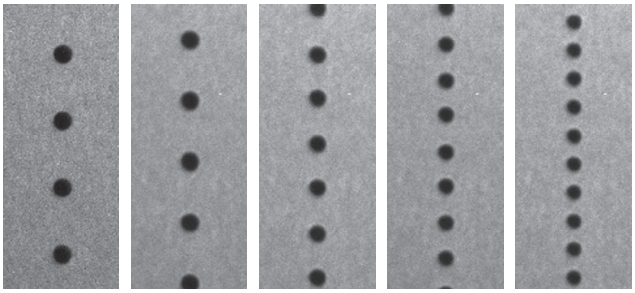

Figure 2. Shadow image of sequences of droplets having the diameter 47, 44, 39, 37 and 33 μm with the repetition rate (a) 40, (b) 60, (c) 80, (d) 100 and (e) 125 kHz, respectively.

In the long-term experiment (more than 1.5 hours) for $n =$ 52 kHz and the droplet diameter 83 μm we managed to achieve the spatial stability of the droplet position with the root-mean-square deviation $\sigma < 1$ μm both in the longitudinal and in the transverse direction. The diameter of droplets was stable during this experiment, $\sigma < 0.3$ μm. In the experiments a few minutes long at different values of n we managed to obtain $\sigma \approx 0.5$ μm. The minimal separation between the droplets in the experiments amounted to ~180 μm, so that for the caustic size of the laser radiation 50 μm the laser beam did not touch the drops adjacent to the target droplet. It was found that the main factors affecting the spatial stability of droplets are the presence of solid-state particles in the melted working substance, as well as the drift of pressure and temperature in the working volume of the droplet generator and nozzle unit. In our experiments, the fineness of the working substance filtering did not exceed 5 μm, and the accuracy of maintaining

the temperature and pressure in the tank was no greater than ±0.1 °C and ±20 mbar, respectively.

3.2. Characteristics of EUV radiation

In the LPP EUV sources based on tin plasma using a CO_2 laser in order to provide efficient generation of radiation near ~13.5 nm, produced by the transitions of ions Sn^{8+}–Sn^{12+}, it is necessary to generate the plasma with the electron temperature ~70 eV, radiating region $n_eL \approx 5 \times 10^{21}$ m^{-2} (n_e is the density of electrons and L is the region length), mean ion charge 10 and ion kinetic energy $E \geqslant 4$ keV [11]. In the LPP source based on a CO_2 laser the region of laser energy absorption, determined by the critical density of electrons (~10^{25} m^{-3}), practically coincides with the region of the EUV radiation emission. This is quite different from the LPP source based on the Nd:YAG laser, where the critical electron density has much larger values (~10^{27} m) and, correspondingly, the region of laser radiation absorption is located significantly nearer to the surface of the target. Therefore, in the latter case in the course of energy transfer from the zone of absorption to the zone of EUV radiation emission, a considerable part of the laser energy is absorbed (in contrast to the case of the CO_2 laser) [11]. This fact partially explains greater values of η for the sources based on CO_2 lasers with the pre-pulse ((4%–5%) $(2\pi\ \mathrm{sr})^{-1}$ [12, 13]) and without pre-pulse (2.8% $(2\pi\ \mathrm{sr})^{-1}$ [14]) as compared to those based on Nd:YAG lasers ((1.5%– 2.5%) $(2\pi\ \mathrm{sr})^{-1}$ [15, 16]).

Figure 3 presents the dependence of the in-band EUV radiation energy on the energy and power density of the laser radiation. Each point is a result of averaging over 100 pulses. One can see that the maximal value of $\eta = 2.3\%$ $(2\pi\ \mathrm{sr})^{-1}$ is achieved at $P_{las} \geqslant 4 \times 10^{11}$ W cm^{-2}. A close value of η for the same P_{las} was achieved in Ref. [16], where the target was a solid-state plate of pure tin, and, in spite of the similar values of P_{las}, it is almost twice as large as η obtained in Ref. [9]. The latter is explained both by a smaller diameter of the target droplet, due to which the most part of laser energy passes beside the target, and by a smaller size of the region where the target droplet interacts with radiation (50 μm in our work against 30 μm in Ref. [9]). According to Ref. [11], this leads to smaller η at the same P_{las}. Therefore, in our case the interaction region is determined by the focal spot diameter, while in Ref. [9] – by the droplet size, i.e., in our work the size of the interaction region is considerably larger than in Ref. [9]. The experiments show that using a target made of eutectic In/Sn alloy one can obtain the energy characteristics of EUV radiation comparable with those for pure tin target.

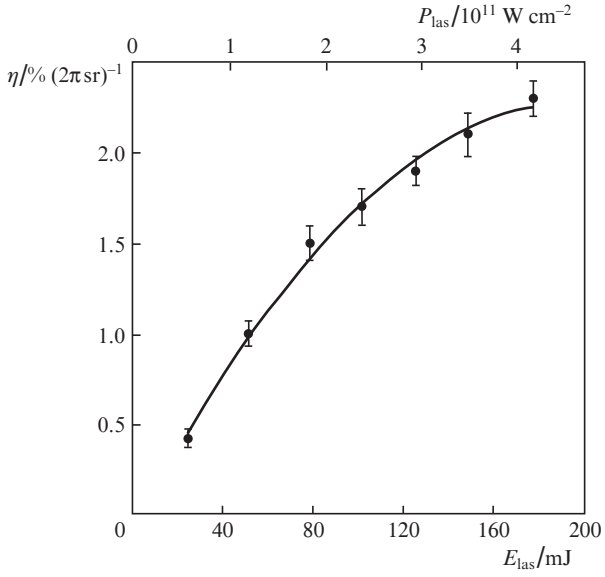

Figure 3. Dependence of η on the energy and power density of laser radiation.

Figure 4 presents the image of the plasma obtained in the EUV range by means of the camera obscura and the CCD camera using the target droplet with the diameter ~80 μm. The size of the radiating plasma at the intensity half-maximum level equalled 82 × 85 μm. The analysis of the image has shown that almost 100% of the EUV energy is emitted from the volume with the radius no greater than 100 μm.

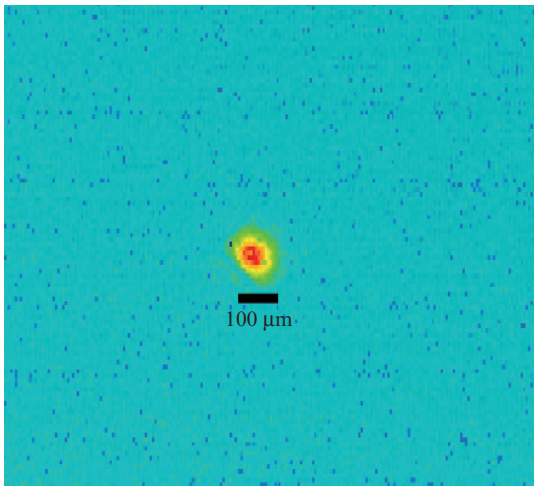

Figure 4. Image of plasma radiating in the EUV range.

Figure 5 shows the spectrum of the laser plasma of the source in the EUV range; the in-band range is also shown. This spectrum is analogous to those obtained in the LPP source using a Nd:YAG laser and pure tin, and strongly differs from than obtained using a CO_2 laser [14], in which the width of the spectrum at the intensity half-maximum level is

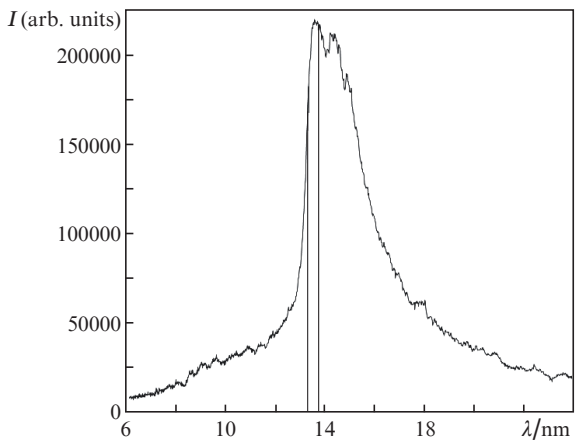

Figure 5. Spectrum of laser plasma radiation from the In/Sn droplet target.

nearly three times smaller than in the case of plasma from the Nd:YAG laser.

3.3. Specific features of repetitively pulsed operation of the EUV source

Figure 6 shows the values of η, obtained for 200 sequential pulses at $f = 10$ Hz. The mean value of η in this experiment amounted to 2.3% $(2\pi\ \mathrm{sr})^{-1}$, the absolute root-mean-square deviation being 0.1%, which corresponds to the relative value $\sigma_0 = 4.3\%$. Though the obtained value of σ_0 is close to the upper boundary of σ_0 values, required for the actinic EUV sources, in our case there is a possibility to reduce it by several times. The point is that the position of the focal spot of the used Nd:YAG laser varies from pulse to pulse due to the instability of the active medium in the direction, perpendicular to the optical axis within the limits ±10 μm, which considerably exceeds the spatial stability of the target droplet position ($\sigma \leqslant 1$ μm). Besides that, the value of σ_0 for the power density of laser radiation from pulse to pulse was no less than 10%. Thus, in our experiments the stability of EUV radiation was mainly determined by the stability of laser parameters.

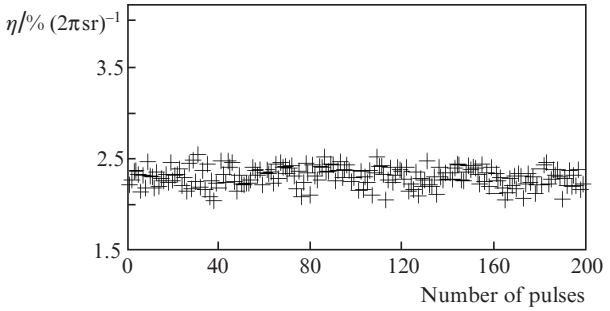

Figure 6. Values of η for the sequence of 200 laser pulses; $f = 10$ Hz.

To simulate the operation of the source at a high repetition rate f and to determine the maximal laser pulse repetition rate f_{max} two experiments were carried out. The plasma and the target droplet fragments can affect the neighbouring droplets and cause their deformation; therefore, in the first experiment f_{max} was determined by detecting the undeformed droplets nearest to the target one. However, this is not sufficient for the determination of f_{max}. One should also assure that the spreading fragments of the target droplet do not shield the radiation of the auxiliary visible-range laser by the reflected signal of which the target droplet and the pointing of the laser radiation are synchronised. That is why the second experiment was performed in which doubled laser pulses separated by a small delay were used to model the operation of the source at high repetition rates. In this case the EUV radiation induced by both laser pulses was recorded.

Figure 7 presents shadow photographs of the droplet at 1.3 μs after the impact of the laser pulse, shot from two directions at the angles 90° and 17° with respect to the optical axis of the laser. The conditions of the experiment were as follows: the drop diameter 83 μm, the repetition rate of droplets 33 kHz, $P_{las} = 2 \times 10^{11}$ W cm^{-2}. The moment of the illuminating laser flash and the duration of the CCD camera frame were chosen such that both the plasma of the target droplet and the dynamics of the droplet deformation at different time instants after the laser pulse could be recorded. In Fig. 7a the focused laser beam propagates from right to left, and in Fig. 7b at the angle 17° to the image plane. The white glow in the centre of the sequence of droplets is the glow of the target plasma, the dark formation to the left from the droplets trajectory in Fig. 7a and the dark circle in Fig. 7b correspond to the deformed target droplet having the shape of a thin disk with bended edges. For the delays longer than 2.3 μs one can observe ruptures appearing at this disk and it begins to break into small fractions. It is easy to estimate that the disk thickness in this case does not exceed 200–250 nm, and the evaporation of the target mass as a result of ablation reduces this thickness.

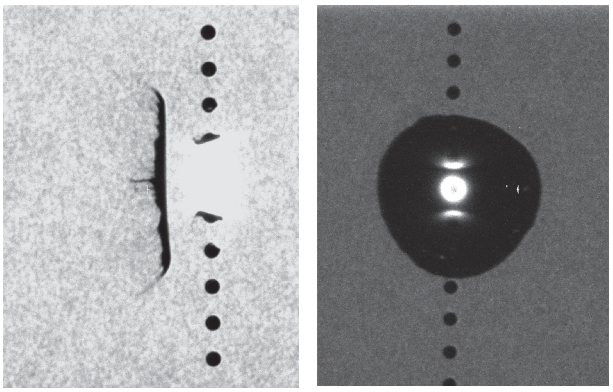

Figure 7. Shadow image of the target droplet deformation, obtained at the angles (a) 90° and (b) 17° with respect to the optical axis of the laser; the droplet diameter is 83 μm, $n = 33$ kHz, and the delay time of the illuminating laser pulse with respect to the main laser pulse is 1.3 μs.

As seen from Fig. 7, the plasma also appears at the surface of the neighbouring droplets, located above and below the target droplet. The image of the interaction region in the EUV range, obtained using the camera obscura, has shown that the plasma at the neighbouring droplets does not emit in this range. Since the laser radiation does not hit the neighbouring droplets, the mechanism of plasma formation of their surfaces due to the EUV radiation and/or the ion flow from the target droplet. In Fig. 7a one can see strong deformation of the neighbouring droplets, caused by the plasma produced at them. Moreover, as shown by the shadow photographs of the interaction region, shot at long delays, the second and sometimes even the third droplet from the target one are subjected to deformation. Thus, this experiment has shown that for the stable operation of the EUV source it is necessary to use at least each fourth, fifth, etc. droplet, i.e., if the repetition rate of the laser pulses $f = 8$ kHz, then the droplet generator should operate with the repetition rate no less than 32 kHz.

The second series of experiments was carried out using the doubled laser system. The small delay time between the pulses of each pair simulated the high pulse repetition rate f. The experiments were performed with the delays, corresponding to $f = 5$, 6, 7, 8 and 10 kHz. Figure 8 shows the shadow photograph of the interaction region with the camera exposure exceeding the pulse repetition period. The pulse repetition rate of the illuminating laser was equal to 5 kHz, the time delay with respect to each pulse of the Nd:YAG laser being

~1.3 μs, so that one frame included the image of both deformed target droplets. As shown by the experiments, the spreading fragments of the droplet do not shield the radiation of the auxiliary laser and do not affect the stability of EUV source operation up to the delays, corresponding to $f \approx 8$ kHz. Figure 9 shows the oscillogram of the EUV signals in the case of modelling the repetitively pulsed operation of the source with $f \approx 8$ kHz. One can see that the amplitudes of the EUV pulses are rather similar, and their difference is due to the instability of laser parameters for each of the lasers, as mentioned above.

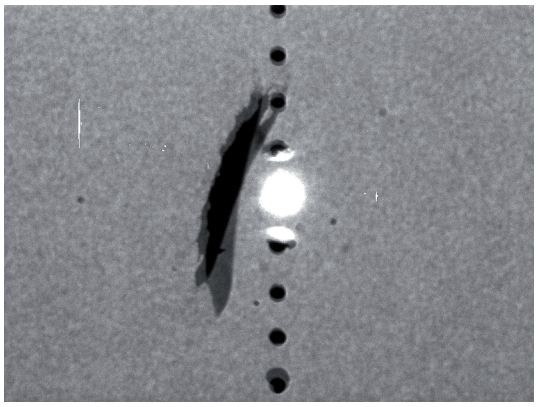

Figure 8. Shadow image of deformed target droplets in the double-pulse regime; the delay between the laser pulses is 200 μs, the delay of the illuminating pulse with respect to the Nd : YAG laser pulse is 1.3 μs.

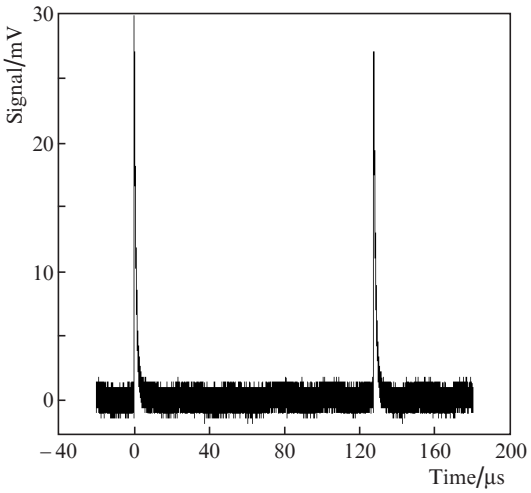

Figure 9. Oscillograms of the EUV signal pulses in the double-pulse regime; the delay between the laser pulses is 125 μs.

For different dimensions and velocities of droplets, the numerical results for both series of experiments will be somewhat different. Most probably, the smaller the droplet diameter and the greater the velocity, the higher the f_{max} value.

The estimate of the source brightness, made on the basis of the above results, has shown a potential possibility of designing a stable source of EUV radiation with the droplet target having the brightness $B = E_{las}\eta f/(2\pi S) \approx 0.96$ kW $(\text{mm}^2\ \text{sr})^{-1}$, where S is the area of radiating plasma. The value of η was assumed to be 2.3%, the laser pulse repetition rate was $f = 8$ kHz, and the rate of droplet generation exceeded 32 kHz. Apparently, a further increase in the brightness in the considered EUV source requires the reduction of the droplet size (no smaller than the focal spot diameter) with a simultaneous increase in the droplets velocity and the repetition rate of laser pulses. The rate of the droplet generation should be such that the plasma and the fragments of the target droplet could affect neither the neighbouring droplets, nor the synchronisation system, triggered by the target droplet.

4. Conclusions

The experimental study of the high-brightness EUV source based on the laser plasma induced by the nanosecond Nd : YAG laser, interacting with a liquid-metal target droplet of eutectic indium–tin alloy was carried out.

To produce the target droplets, a stable droplet generator was developed based on the principle of the forced capillary jet decomposition, with a low-temperature working substance that allows an increase in reliability and lifetime. The repetition rate of the droplets, their size and velocity can be varied within the ranges 20–125 kHz, 30–100 μm and 6–15 m s^{-1}, respectively. For the target droplets the spatial stability of the centre-of-mass position $\sigma < 1$ μm at 45 mm from the nozzle was achieved during 1.5 hours of the droplet generator operation. For the power density at the target droplet 4×10^{11} W cm^{-2} the mean efficiency of conversion of the laser energy into that of the EUV radiation in the range 13.5 ± 0.135 nm was equal to $2.3\%\,(2\pi\,\text{sr})^{-1}$, the diameter of the radiating plasma being 83 μm. It was shown that the EUV radiation spectrum is close to the laser plasma spectrum of tin. The effect of fragments of the target droplet on the deformation of neighbouring droplets was studied. The physical factors that limit the maximal repetition rate of the source pulses were revealed. The experimental modelling of the repetitively pulsed operation regime has shown that it can be stable at the pulse repetition rate up to 8 kHz and the droplets repetition rate above 32 kHz, which will allow the achievement of high mean brightness of the source [~0.96 kW $(\text{mm}^2\ \text{sr})^{-1}$]. The proposed actinic EUV source can be used for the mask diagnostics in the projection EUV lithography.

Acknowledgements. The work was supported by the RF Ministry of Education and Science [Agreement No. 4.579.21.0004, unique identifier of applied research (project) RFMEFI57914X0004].

References

1. Bakshi V. (Ed.) *EUV Source for Lithography* (Bellingham, Wash.: SPIE Press, 2006).
2. Tallents G., Wagenaars E., Pert G. *Nature Photon.*, **4**, 809 (2010).
3. Choi P., Zakharov S., Aliaga-Rossel R., Bakouboula A., Benali O., Bove P., Michele G., Duffy G., Iwase O., Lebert B., Powell K., Sarroukh O., Zaepffel C., Zakharov V. *J. Micro/Nanolith. MEMS MOEMS*, **11** (2), 021107 (2012).
4. Vinokhodov A.Yu., Krivtsun V.M., Lash A.A., Borisov V.M., Yakushev O.F., Koshelev K.N. *Kvantovaya Elektron.*, **46** (1), 81 (2016) [*Quantum Electron.*, **46** (1), 81 (2016)].
5. Hansson B.A.M., Fomenkov I.V., Böwering N.R., Ershov A.I., Partlo W.N., Myers D.W., Khodykin O.V., Bykanov A.N., Rettig C.L., Hoffman J.R., Vargas L.E., Simmons R.D., Chavez J.A., Marx W.F., Brandt D.C. *Proc. SPIE Int. Soc. Opt. Eng.*, **6151**, 61510R (2006).
6. Tomie T. *J. Micro/Nanolith. MEMS MOEMS*, **11** (2), 021109 (2012).

7. Teramotoa Y., Santosa B., Mertensa G., Kopsa R., Kopsa M., Küpperb F., Niimic G., Yabutac H., Naganoc A., Yokoyamac T., Yoshiokac M., Shiraic T., Ashizawac N., Satoc H., Nakamurac K., Kasamac K. *Proc. SPIE Int. Soc. Opt. Eng*., **9048**, 904813 (2014).
8. Mizoguchi H., Nakarai H., Abe T., Ohta T., Nowak K.M., Kawasuji Y., Tanaka H., Watanabe Y., Hori T., Kodama T., Shiraishi Y., Yanagida T., Yamada T., Yamazaki T., Okazaki S., Saitou T. *Proc. SPIE Int. Soc. Opt. Eng*., **9048**, 90480D (2014).
9. Rollinger B., Gambino N., Giovannini A.Z., Bozinova L.S., Alickaj F., Hertig K., Abhari R.S. *Proc. SPIE Int. Soc. Opt. Eng*., **9048**, 90482K1-9 (2014).
10. Vinokhodov A.Yu., Koshelev K.N., Krivtsun V.M., Krivokorytov M.S., Sidelnikov Yu.V., Medvedev S.V., Kompanets V.O., Melnikov A.A., Chekalin S.V. *Kvantovaya Elektron*., **46** (1), 23 (2016) [*Quantum Electron*., **46** (1), 23 (2016)].
11. Banine V.Y., Koshelev K.N., Swinkels G.H.P.M. *J. Phys. D: Appl. Phys*., **44**, 253001 (2011).
12. Mizoguchi H., Nakarai H., Abe T., Ohta T., Nowak K.M., Kawasuji Y., Tanaka H., Watanabe Y., Hori T., Kodama T., Shiraishi Y., Yanagida T., Soumagne G., Yamada T., Yamazaki T., Okazaki S., Saitou T. *Proc. Int. EUVL Symposium* (Maastricht, Netherland, 2015).
13. Fujimoto J., Hori T., Yanagida T., Mizoguchi H. *Hindawi Phys. Res. Intern.*, **2012**, Article ID 249495 (2012).
14. Abe N., Sumitani A., Sato H., Mizoguchi H., Endo A., Toyoda K. *Proc. SEMATECH Litho Forum* (Vancouver, Canada, 2006).
15. Hoffman J.R., Bykanov A.N., Khodykin O.V., Ershov A.I., Böwering N.R., Fomenkov I.V., Partlo W.N., Myers D.W. *Proc. SPIE Int. Soc. Opt. Eng*., **5751**, 892 (2005).
16. Coons R.W., Campos D., Crank M., Harilal S.S., Hassanein A. *Proc. SPIE Int. Soc Opt. Eng*., **7636**, 763636 (2010).